Proceedings of the ASME 2009 Dynamic Systems and Control Conference
DSCC2009
October 12-14, 2009, Hollywood, California, USA

DSCC2009-2736

HYBRID ADAPTIVE FRICTION COMPENSATION OF INDIRECT DRIVE TRAINS *

Wenjie Chen
Dept. of Mechanical Engineering
University of California
Berkeley, California 94720
Email: wjchen@me.berkeley.edu

Kyoungchul Kong
Dept. of Mechanical Engineering
University of California
Berkeley, California 94720
Email: kckong@me.berkeley.edu

Masayoshi Tomizuka
Dept. of Mechanical Engineering
University of California
Berkeley, California 94720
Email: tomizuka@me.berkeley.edu

ABSTRACT

This paper investigates the friction compensation topic for indirect drive trains in the absence of precise end-effector measurements. Friction, one of the main factors that diminish control performance, is investigated and compensated by manipulating the reference trajectory as well as the torque input. The motor side torque compensation utilizes the modified LuGre model to design an adaptive friction observer, while the motor side reference is modified by injecting the estimated load side friction. A hybrid controller structure is proposed to engage or disengage the load side compensator. Both methods are combined to effectively reject the friction effects in indirect drive trains. The effectiveness of the proposed scheme is experimentally verified.

INTRODUCTION

Indirect drive trains, e.g., robotic joints that utilize gear transmissions, are commonly used in industrial applications due to the high torque capacity. The indirect gear transmissions, however, set challenges in high precision motion control because of gear compliances and nonlinearities such as friction and torque hysteresis. Particularly, the nonlinear friction effects on the load side are difficult to compensate for, because: 1) precise load side measurement is often unavailable, and 2) it is indirectly actuated through the gear transmission. Since the load side performance is critical in practical applications, a method that compensates for friction on the load side as well as the motor side is necessary.

Over the past several decades, modeling and compensation of the friction effects have been intensively studied from various viewpoints, including static/dynamic characterizations and feedback/feedforward compensation schemes [1, 2]. For example, many model-based friction compensation techniques have been developed to reject the friction effects by adaptively [3] and robustly [4] observing the real friction. Also, typical approaches, such as the disturbance observer [5] or repetitive control [6], have been used to compensate for friction.

Most of these studies, however, verified their performance based on simple one-mass systems or direct drives only. When a two-mass system or an indirect drive is considered, the friction effects introduced from the load side remain a challenge. For this reason, friction characteristics in harmonic drive systems were studied in [7,8]. The performance and stability issues due to friction forces (e.g., limit cycles) were addressed in [9]. Some compensation schemes were proposed to overcome the friction effects in harmonic drives. Most of them, however, focused on the motor side compensation only [8] or torque tracking control [10]. To improve the load side position tracking performance, the position measurements of both motor side and load side have been utilized in the controller design [11]. Such controllers, however, are difficult to implement in industrial robots, which are usually not equipped with sensors for load side position measurement.

In this paper, a friction compensation scheme for indirect drive trains is developed in the absence of precise load side measurements. The proposed method manipulates both the torque input and the reference trajectory, which is controlled by a hybrid system scheme based on the tracking performance. The effectiveness of the method is verified by experimental results.

SYSTEM OVERVIEW

Single-Joint Indirect Drive Model

Figure 1 shows the schematic of a single-joint indirect drive mechanism. The subscripts m and ℓ denote the motor side and

*THIS WORK WAS SUPPORTED BY FANUC LTD., JAPAN. REAL-TIME CONTROL HARDWARE AND SOFTWARE WERE PROVIDED BY NATIONAL INSTRUMENTS, INC.

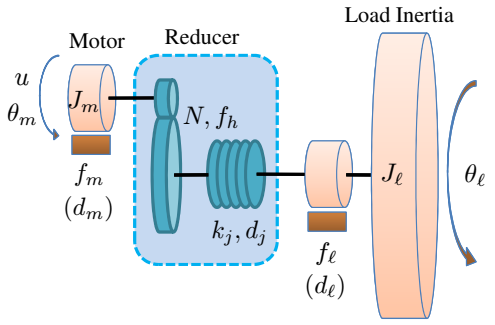

Figure 1. SINGLE-JOINT INDIRECT-DRIVE MECHANISM

the load side quantities, respectively. d represents the viscous damping coefficient, and J is the moment of inertia. θ and u represent the angular position and motor torque output, respectively. k_j and d_j are the linear stiffness and the viscous damping coefficients of the reducer. The gear ratio of the reducer is denoted by N. f_m, f_ℓ, and f_h represent the nonlinear friction forces at the motor side, the load side, and the reducer, respectively. Note that f_m and f_ℓ include the viscous damping effects d_m and d_ℓ, respectively. These friction forces are further discussed later.

Equations of motion for the system in Fig. 1 are

$$J_m\ddot{\theta}_m + f_m + f_h = u - \frac{1}{N}\left[k_j\left(\frac{\theta_m}{N} - \theta_\ell\right) + d_j\left(\frac{\dot{\theta}_m}{N} - \dot{\theta}_\ell\right)\right] \quad (1)$$

$$J_\ell\ddot{\theta}_\ell + f_\ell = k_j\left(\frac{\theta_m}{N} - \theta_\ell\right) + d_j\left(\frac{\dot{\theta}_m}{N} - \dot{\theta}_\ell\right) \quad (2)$$

Friction Model

In the system shown in Fig. 1, the energy is dissipated mainly by three friction forces: the motor bearing friction, f_m, the load output bearing friction, f_ℓ, and the harmonic drive gear meshing friction, f_h. Although the gear meshing friction f_h is dominant in a free load condition [7], the load side friction f_ℓ can become more significant as the load side inertia increases.

The combination of system model (1)-(2) gives

$$J_m\ddot{\theta}_m + \frac{1}{N}J_\ell\ddot{\theta}_\ell = u - F \quad (3)$$

where $F = f_m + f_h + \frac{f_\ell}{N}$ can be explained as the entire friction force imposed on the whole system referred to the motor side.

There are several reasons to model the entire friction force F as reflected on the motor side. First of all, it is easier to identify the friction on the motor side for industrial indirect drives. Furthermore, from the torque compensation point of view, the friction force is usually compensated at the motor side where the actuator is. Also it is not necessary to model these friction forces separately, especially when they exhibit similar behaviors.

To describe the entire friction force F, this paper employs the Lund-Grenoble (LuGre) model [1]. The LuGre model uses an internal friction state, z, governed by

$$\dot{z} = v - \frac{\beta_0|v|}{g(v)}z \quad (4)$$

$$g(v) = F_c + (F_s - F_c)\,e^{(-v^2/v_s^2)} \quad (5)$$

$$F = \sigma_0 z + \sigma_1\dot{z} + \sigma_2 v \quad (6)$$

where v is the relative velocity between the two contacting surfaces at the motor side, i.e., $v = \dot{\theta}_m$. σ_0, σ_1, and σ_2 represent the micro-stiffness, micro-damping of the internal state z, and the macro-damping of the velocity v, respectively. The function $g(v)$ is chosen to capture the Stribeck effect, where F_C and F_S are the levels of Coulomb friction and stiction force, respectively. v_s is the Stribeck velocity. The internal friction state z can be regarded as the deflection of bristles, which represents the asperities between the two contacting surfaces.

In Eq. (4), note that an additional parameter, β_0, is used to define the nominal micro-stiffness of the internal state z, which differs from the standard LuGre model. This modification will simplify the friction compensation algorithm.

Equations (4)-(6) give the entire friction force, F, as

$$F = K^{\mathrm{T}}\Phi \quad (7)$$

where $K = \left[\sigma_1 + \sigma_2 \;\; \sigma_0 \;\; \beta_0\sigma_1\right]^{\mathrm{T}}$, $\Phi = \left[v \;\; z \;\; -\frac{|v|}{g(v)}z\right]^{\mathrm{T}}$.

Notice that the modified LuGre model still preserves the following property of standard LuGre model [1]:

Property 1. *$F_c \le g(v) \le F_s$. $|z(t)| \le \frac{F_s}{\beta_0}$, $\forall t \ge 0$ if $|z(0)| \le \frac{F_s}{\beta_0}$.*

In reality, it can be assumed that the deflection of bristles starts at rest, i.e., $z(0) = 0$. Therefore, $|z(t)| \le \frac{F_s}{\beta_0}, \forall t \ge 0$. This property will be used in the subsequent controller design to ensure the bounded stability of the friction observer.

In practice, friction characteristics may vary due to the variations of the normal forces in contact, lubricant condition, temperature, material wear, etc. [3] Variations in the normal forces usually cause an impact only on the static parameters, i.e., F_C, F_S, v_s, and σ_2, while the changes in lubricant condition, temperature and/or materials may affect both static and dynamic parameters.

By fixing the nominal micro-stiffness, β_0, the adaptation of real micro-stiffness, σ_0, effectively changes the level of static parameters, i.e., F_C, F_S, and v_s in $g(v)$. Thus, the adaptation of σ_0, σ_1, and σ_2 can account for most parameter variations in the modified friction model, even if the dynamics of internal state z does not strictly follow Eq. (4). Therefore, σ_0, σ_1, and σ_2 are the parameters to be adapted in the proposed algorithm, i.e., K is to be updated in real time, and Φ is the regressor.

In the case that the load side friction effects are not negligible, it is necessary to consider the load side friction separately. Assuming that the load side friction shares the same characteristics as the entire friction force, F, a ratio r_ℓ can be introduced to

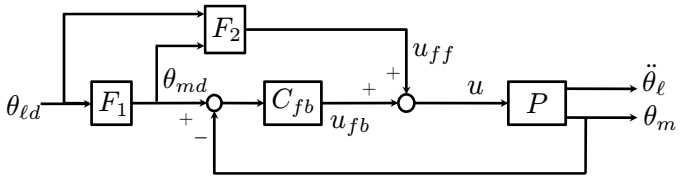

Figure 2. BLOCK DIAGRAM OF THE OVERALL CONTROL SYSTEM

derive the load side friction f_ℓ from F, i.e.

$$f_\ell = r_\ell F \tag{8}$$

This assumption is reasonable in most cases, especially when the motor is spinning in one direction. The transient behavior during the velocity reversal may not strictly follow the assumption. This velocity reversal case, however, is not of the interest in most applications since the transient time is usually sufficiently short to be negligible.

Controller Structure

Figure 2 shows the overall control structure of the single-joint indirect drive system. It consists of two feedforward controllers, F_1 and F_2, and one feedback controller, C_{fb}.

The feedforward controller, F_2, is designed as

$$u_{ff}(t) = J_m \ddot{\theta}_{md}(t) + \frac{1}{N} J_\ell \ddot{\theta}_{\ell d}(t) + \hat{F}(t) \tag{9}$$

where $\hat{F}$ is the estimated entire friction force. $\ddot{\theta}_{\ell d}$ is the desired load side acceleration. In the case that the acceleration is measured by sensors (e.g., load side accelerometers), $\ddot{\theta}_{\ell d}$ can be replaced with $\ddot{\theta}_\ell$. θ_{md} is the motor side position reference generated by F_1 from the desired load side position, $\theta_{\ell d}$, i.e.

$$\theta_{md}(t) = \frac{N}{k_j}\left[J_\ell \ddot{\theta}_{\ell d}(t) + \hat{f}_\ell(t)\right] + N\theta_{\ell d}(t) \tag{10}$$

where $\hat{f}_\ell$ is the estimated load side friction, and $\ddot{\theta}_{\ell d}$ is the second derivative of $\theta_{\ell d}$. Equation (10) is derived from Eq. (2) by neglecting the joint damping d_j, since $k_j\left(\frac{\theta_m}{N} - \theta_\ell\right) \gg d_j\left(\frac{\dot{\theta}_m}{N} - \dot{\theta}_\ell\right)$ usually holds within the system bandwidth range.

The feedback controller, C_{fb}, which consists of a proportional position control loop and a proportional-integral (PI) velocity control loop, can be described as

$$C_{fb}(s) = \left(k_v + \frac{k_i}{s}\right)(s + k_p) \tag{11}$$

where k_p is the gain of the position loop, k_v and k_i are the gains of the velocity loop. The above controller is discretized by the Euler method for implementation.

FRICTION COMPENSATION

As shown in the controller structure (i.e., Eqs. (9)-(10)), the proposed friction compensator consists of two parts. The motor side friction compensation is designed into feedforward controller F_2 by injecting the torque input, and the load side friction effects are further compensated in feedforward controller F_1 by manipulating the motor side reference, θ_{md}.

Motor Side Friction Compensation

Feedback Friction Compensation Let $e_m = \theta_m - \theta_{md}$ be the motor side position tracking error. Define a first order sliding surface, p_m, as

$$p_m = \dot{e}_m + k_s e_m \tag{12}$$

where k_s is a positive constant. Note that e_m is small or converges to zero if p_m is small or converges to zero, since $\frac{e_m(s)}{p_m(s)} = \frac{1}{s+k_s}$ is asymptotically stable.

From Eqs. (3) and (12), the motor side error dynamics is derived as

$$J_m \dot{p}_m = u - F - \frac{1}{N} J_\ell \ddot{\theta}_\ell - J_m \ddot{\theta}_{md} + J_m k_s \dot{e}_m \tag{13}$$

The controller structure yields the following control law

$$\begin{aligned} u(t) &= u_{ff}(t) + u_{fb}(t) \\ &= \left[J_m \ddot{\theta}_{md}(t) + \frac{1}{N} J_\ell \ddot{\theta}_{\ell d}(t) + \hat{F}(t)\right] - \left[k_v s_m(t) + \int_0^t k_i s_m(\tau) d\tau\right] \end{aligned} \tag{14}$$

where $s_m(t) = \dot{e}_m(t) + k_p e_m(t)$ is the error term in the velocity loop.

By applying the adaptive control technique, an adaptive friction observer is designed to obtain $\hat{F}(t)$, i.e.

$$\hat{F} = \hat{K}^{\mathrm{T}} \hat{\Phi} \tag{15}$$

where $\hat{\Phi} = \left[\dot{\theta}_m \;\; \hat{z}_0 \;\; -\frac{|\dot{\theta}_m|}{g(\dot{\theta}_m)}\hat{z}_1\right]^{\mathrm{T}}$. $\hat{K}$, $\hat{z}_0$, and $\hat{z}_1$ are the estimates obtained from the following update laws:

$$\dot{\hat{K}} = -\Gamma \hat{\Phi} p_m \tag{16}$$

$$\dot{\hat{z}}_0 = \dot{\theta}_m - \frac{\beta_0 |\dot{\theta}_m|}{g(\dot{\theta}_m)} \hat{z}_0 - \gamma_3 p_m \tag{17}$$

$$\dot{\hat{z}}_1 = \dot{\theta}_m - \frac{\beta_0 |\dot{\theta}_m|}{g(\dot{\theta}_m)} \hat{z}_1 + \gamma_4 \frac{|\dot{\theta}_m|}{g(\dot{\theta}_m)} p_m \tag{18}$$

where $\Gamma = \mathrm{diag}(\gamma_0, \gamma_1, \gamma_2)$, γ_3 and γ_4 are positive adaptation gains. Notice that the unmeasurable internal friction state z is

estimated by a dual-observer structure [12] with the two state estimates, $\hat{z}_0$ and $\hat{z}_1$. Equations (17) and (18) result in the following observer error dynamics:

$$\dot{\tilde{z}}_0 = -\frac{\beta_0 \left|\dot{\theta}_m\right|}{g\left(\dot{\theta}_m\right)}\tilde{z}_0 + \gamma_3 p_m \tag{19}$$

$$\dot{\tilde{z}}_1 = -\frac{\beta_0 \left|\dot{\theta}_m\right|}{g\left(\dot{\theta}_m\right)}\tilde{z}_1 - \gamma_4 \frac{\left|\dot{\theta}_m\right|}{g\left(\dot{\theta}_m\right)} p_m \tag{20}$$

where $\tilde{z}_0 = z - \hat{z}_0$ and $\tilde{z}_1 = z - \hat{z}_1$.

Stability Analysis The following theorem proves the stability of the closed-loop system under additional assumptions as stated therein.

Theorem 1. *For the system model described by Eqs.* (1)-(6)*, global asymptotic tracking performance on the motor side can be achieved by the proposed controller in Eqs. (9)-(11) and adaptive friction observer in Eqs. (15)-(18), if the integrator term of the feedback controller, C_{fb}, is suppressed, i.e., $k_i = 0$, and the real load side acceleration measurement, $\ddot{\theta}_\ell$, is used in Eq. (9).*

Proof. Suppose that the feedback controller gains are

$$k_p = \frac{h k_s}{J_m k_s + h}, \quad k_v = J_m k_s + h \tag{21}$$

where h is a positive constant. By the assumption in the theorem, $k_i = 0$. Then the control law in Eq. (14) can be rewritten as

$$u = \left[J_m \ddot{\theta}_{md} + \frac{1}{N} J_\ell \ddot{\theta}_{\ell d} + \hat{F} \right] - \left[J_m k_s \dot{e}_m + h p_m \right] \tag{22}$$

From Eqs. (13) and (22), the control law results in the following closed loop dynamics

$$\begin{aligned} J_m \dot{p}_m &= -h p_m - \frac{J_\ell}{N}\left(\ddot{\theta}_\ell - \ddot{\theta}_{\ell d}\right) - \left(F - \hat{F}\right) \\ &= -h p_m - \frac{J_\ell}{N}\ddot{e}_\ell - \tilde{K}^{\mathrm{T}}\hat{\Phi} - K^{\mathrm{T}}\tilde{\Phi} \end{aligned} \tag{23}$$

where $\ddot{e}_\ell = \ddot{\theta}_\ell - \ddot{\theta}_{\ell d}$ is the load side acceleration tracking error, $\tilde{K} = K - \hat{K}$ and $\tilde{\Phi} = \Phi - \hat{\Phi}$ are the estimation errors.

Let a Lyapunov function candidate for the system be

$$V = \frac{1}{2} J_m p_m^2 + \frac{1}{2}\tilde{K}^{\mathrm{T}} \mathrm{diag}(\gamma_0, \gamma_1, \gamma_2)^{-1} \tilde{K} + \frac{1}{2\gamma_3} k_1 \tilde{z}_0^2 + \frac{1}{2\gamma_4} k_2 \tilde{z}_1^2 \tag{24}$$

where $k_1 = \sigma_0$ and $k_2 = \beta_0 \sigma_1$ are the last two entries in K.

In most applications, it is reasonable to assume that the actual friction parameters, $K = \left[\sigma_1 + \sigma_2 \;\; \sigma_0 \;\; \beta_0 \sigma_1\right]^{\mathrm{T}}$, are unknown but constant. It follows that $\dot{K} = \mathbf{0}$ and $\dot{\tilde{K}} = -\dot{\hat{K}}$. Therefore, differentiating V in Eq. (24) and substituting the update laws from Eqs. (16)-(18), the derivative of V is obtained as

$$\dot{V} = -h p_m^2 - \frac{J_\ell}{N} p_m \ddot{e}_\ell - \frac{k_1}{\gamma_3} \frac{\beta_0 \left|\dot{\theta}_m\right|}{g\left(\dot{\theta}_m\right)} \tilde{z}_0^2 - \frac{k_2}{\gamma_4} \frac{\beta_0 \left|\dot{\theta}_m\right|}{g\left(\dot{\theta}_m\right)} \tilde{z}_1^2 \tag{25}$$

Recall that h is a positive constant. Thus, every term on the right hand side of Eq. (25), except for the second term, is negative semi-definite. Moreover, if the load side acceleration is measured by sensors (i.e., $\ddot{\theta}_{\ell d}$ is replaced with $\ddot{\theta}_\ell$ in u_{ff} in Eq. (9)), the second term becomes zero. It follows that

$$\dot{V} = -h p_m^2 - \frac{k_1}{\gamma_3} \frac{\beta_0 \left|\dot{\theta}_m\right|}{g\left(\dot{\theta}_m\right)} \tilde{z}_0^2 - \frac{k_2}{\gamma_4} \frac{\beta_0 \left|\dot{\theta}_m\right|}{g\left(\dot{\theta}_m\right)} \tilde{z}_1^2 \leq -h p_m^2 \tag{26}$$

From Lyapunov stability theory, it is concluded that the motor side tracking error, p_m, the friction parameter estimation errors, $\tilde{K}$, and the internal friction state estimation errors, $\tilde{z}_0$ and $\tilde{z}_1$, are globally uniformly bounded. Since the actual friction parameters K are constant during one trajectory task, and actual internal friction state, z, is bounded as shown in Property 1, it follows that the estimates, $\hat{K}$, $\hat{z}_0$, and $\hat{z}_1$, are globally uniformly bounded as well. In addition, the actual motor side position and velocity, θ_m and $\dot{\theta}_m$, are globally uniformly bounded since the generated motor side references are bounded by the characteristics of the feedforward controller, F_1. Equations (24) and (26) also imply that $p_m \to 0$ as $t \to \infty$. Therefore, the motor side tracking error e_m asymptotically converges to zero.

The above theorem provides a sufficient condition to achieve global asymptotic tracking performance on the motor side. Two assumptions were introduced to theoretically guarantee the stability of the proposed method. These assumptions, however, may be relaxed without jeopardizing the closed loop stability of the system in practice. The relaxation is demonstrated in the experiments with preserved integrator in C_{fb} to maintain the basic feedback controller structure (i.e., $k_i \neq 0$). Also, the desired reference $\ddot{\theta}_{\ell d}$ is used in Eq. (9) instead of the real measurement $\ddot{\theta}_\ell$ to attenuate the dependence on the sensors from the load side.

Feedforward Friction Compensation The above friction compensation scheme is in the feedback form, since the actual physical measurements are used in the regressor estimate, $\hat{\Phi}$. When doing tracking control, feedforward control often improves the performance in the sense that it allows anti-causal terms in the controller. It recovers the limitation of feedback controller due to the dynamic lag of the plant. Recall that the feedback controller must see an error first before it can take any corrective action. In particular, this limitation affects the performance by the quick direction reversal of Coulomb friction force.

By replacing the measurements in the friction observer with corresponding desired trajectory profile, excluding the motor side error term, p_m, a feedforward version of the proposed compensation scheme is obtained, where $\hat{\Phi}$ and $\hat{z}$ are modified as

$$\hat{\Phi}_d = \left[\dot{\theta}_{md} \;\; \hat{z}_d \;\; -\frac{|\dot{\theta}_{md}|}{g(\dot{\theta}_{md})}\hat{z}_d\right]^{\mathrm{T}}, \quad \dot{\hat{z}}_d = \dot{\theta}_{md} - \frac{\beta_0 |\dot{\theta}_{md}|}{g(\dot{\theta}_{md})}\hat{z}_d \quad (27)$$

In this form, the dual estimations of internal friction state z are replaced by single desired (nominal) internal state $\hat{z}_d$ as in Eq. (27). Note that Eq. (27) uses desired trajectory without the feedback correction term, p_m. In this feedforward form, the friction observer structure is simplified by reducing the number of adaptive variables from 5 to 3, and the noises and disturbances from feedback measurements are also avoided.

Load Side Friction Compensation

Due to the characteristics of indirect drives, perfect tracking performance on the motor side does not guarantee perfect load side tracking performance. Since the load side performance is of the most interest in practical applications, it is necessary to apply friction compensation as in Eq. (10) to achieve desired performance objectives on the load side.

In Eq. (8), the load side friction, f_ℓ, is modeled as a scaled quantity of the entire friction force, F. Thus, once friction parameters are adapted successfully on the motor side, the load side friction f_ℓ can be estimated as

$$\hat{f}_\ell = \hat{r}_\ell \hat{F} \quad (28)$$

where $\hat{F}$ is the estimated entire friction force from the motor side friction compensator, and $\hat{r}_\ell$ is the estimated scaling factor obtained by the following update laws:

$$\dot{\hat{r}}_\ell = -\gamma_{r_\ell} \hat{F} \hat{e}_\ell, \quad \hat{e}_\ell = \hat{\theta}_\ell - \theta_{\ell d} \quad (29)$$

where $\gamma_{r_\ell} > 0$ is the adaptation gain, $\hat{\theta}_\ell$ is the estimated load side position produced by some estimation algorithm, such as the extended kinematic model based Kalman filter with accelerometers and gyroscope (KKF-AG) described in [13].

Hybrid Compensator Structure

Since the load side friction estimate, $\hat{f}_\ell$, is injected into the motor side reference, θ_{md}, it is desired that the compensated reference is still smooth and continuously differentiable, since the motor side velocity reference, $\dot{\theta}_{md}$, is needed in the feedback controller, C_{fb}. To ensure this, the load side compensation should be active only when the friction parameters in the motor side compensator have converged to some sub-optimal values and then set fixed (i.e., $\Gamma = \mathbf{0}$). This leads to the following hybrid compensator structure.

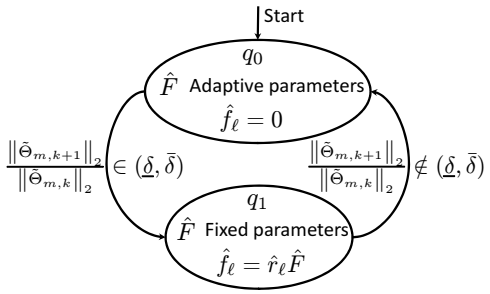

Figure 3. HYBRID COMPENSATOR STRUCTURE

Figure 3 shows the hybrid compensator structure. q_0 and q_1 are the two discrete controller states of the hybrid compensator. In industrial applications, the same task is usually executed repeatedly. Define $\|\tilde{\Theta}_{m,k}\|_2$ as the two-norm of the motor side position tracking error in the k-th execution of the same task, i.e.

$$\|\tilde{\Theta}_{m,k}\|_2 = \left(\sum_{i=1}^{n} |\tilde{\theta}_{m,k}(i)|^2\right)^{\frac{1}{2}} \quad (30)$$

where $\tilde{\theta}_{m,k}(i) = \theta_{m,k}(i) - \theta_{md}(i)$ is the motor side position tracking error at the i-th time step in the k-th execution of the same task, and n defines the duration of each execution.

The controller starts from the state q_0, where the adaptive motor side compensator is activated, and the load side compensator is disabled (i.e., $\hat{f}_\ell = 0$). If $\frac{\|\tilde{\Theta}_{m,k+1}\|_2}{\|\tilde{\Theta}_{m,k}\|_2} \in (\underline{\delta}, \bar{\delta})$, where $(\underline{\delta}, \bar{\delta})$ is the convergence boundary, the compensator scheme is switched to the state q_1. This means that the friction adaptation in the motor side compensator has reached its sub-optimal stage, and cannot significantly improve the motor side tracking performance. At this stage, the load side compensator is enabled while the friction parameters in the motor side compensator are fixed.

If $\frac{\|\tilde{\Theta}_{m,k+1}\|_2}{\|\tilde{\Theta}_{m,k}\|_2} \notin (\underline{\delta}, \bar{\delta})$, the motor side tracking performance can be further improved by adapting the parameters in the motor side compensator. Thus, the compensator scheme is switched back to the initial state q_0.

EXPERIMENTAL RESULTS

Experimental Setup

The proposed friction compensation method is applied to a single-joint indirect drive system shown in Fig. 4. The experimental setup consists of 1) a servo motor with a 20,000 counts/revolution encoder, 2) a harmonic drive with a 80:1 gear ratio, 3) a load-side 144,000 counts/revolution encoder, 4) and a payload. The anti-resonant and resonant frequencies of the setup are about 11Hz and 19Hz. A MEMS gyroscope (Analog, Type: ADXRS150) is installed at one end of the payload and two accelerometers (Kistler, Type: 8330A3) are installed at the ends of

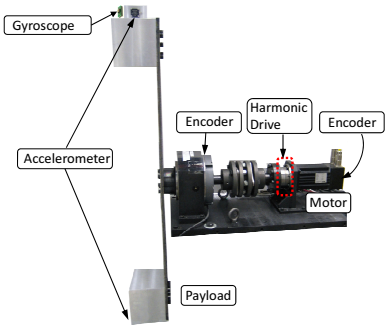

Figure 4. SINGLE-JOINT INDIRECT DRIVE SYSTEM SETUP

the payload symmetrically as shown in Fig. 4. The load side encoder is only for performance evaluation. Also, the accelerometers and gyroscope are only for load side information estimation, not directly for friction compensation algorithms; e.g., $\ddot{\theta}_{\ell d}$ is used in Eq. (9), since it does not practically influence the stability in the experiments. Finally, the controller is implemented in a LabVIEW real-time target installed with LabVIEW Real-Time and FPGA modules. The sampling rate is selected as 1 kHz.

Friction Identification

Friction identification is conducted to set initial values in the adaptive friction observer. The steady state friction regime (gross motion) is characterized by $\dot{z} = 0$, $\ddot{\theta}_m = 0$, and $\ddot{\theta}_\ell = 0$ [2]. Thus, the model in Eqs. (1)-(6) is reduced to the static relation

$$u = F\left(\dot{\theta}_m\right) = \left[F_c + (F_s - F_c)\, e^{\left(-\dot{\theta}_m^2/v_s^2\right)}\right] \operatorname{sgn}\left(\dot{\theta}_m\right) + \sigma_2 \dot{\theta}_m \quad (31)$$

This nonlinear function properly describes a static velocity-torque (friction force) characteristic, as shown in Fig. 5.

Each point in Fig. 5 is obtained by keeping the motor side velocity constant for the same amount of distance in a closed-loop manner. The average value of the steady state torque (friction force $F\left(\dot{\theta}_m\right)$) at the corresponding velocity is recorded. The experiment is repeated at various velocities for the same path to obtain the whole static velocity-torque map. The nonlinear least squares method in the Optimization Toolbox of MATLAB is applied to obtain the static friction parameters, F_C, F_S, v_s, and σ_2.

It is shown in [2] that the dynamic parameters, σ_0 and σ_1, can be identified using an ARX (AutoRegressive with eXtra input signal) or a BJ (Box Jenkins) model structure with pre-sliding motion data. The resolution of the motor encoder, however, limits the implementation of this method. Thus, the method in [3] is employed here to obtain the rough estimate of σ_0, using ramp and step input response data, which gives $\hat{\sigma}_0 = 33.34$(ramp) and 57.03(step) Nm·rad^{-1}, respectively. Note that, the identification of σ_1 is still not available due to the lack of a high resolution encoder. This problem can be solved by using the proposed compensation scheme, since σ_0 and σ_1 are adapted in real time.

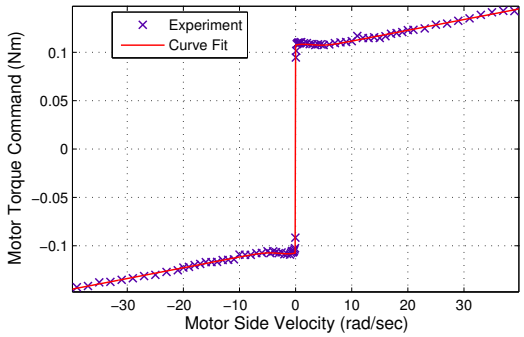

Figure 5. STATIC FRICTION IDENTIFICATION RESULT

Table 1. THE IDENTIFIED FRICTION PARAMETERS (SI UNITS)

$\hat{F}_c$	$\hat{F}_s$	$\hat{v}_s$	$\hat{\sigma}_0$	$\hat{\sigma}_1$	$\hat{\sigma}_2$
0.1004	0.1075	3.951	40	0	0.001114

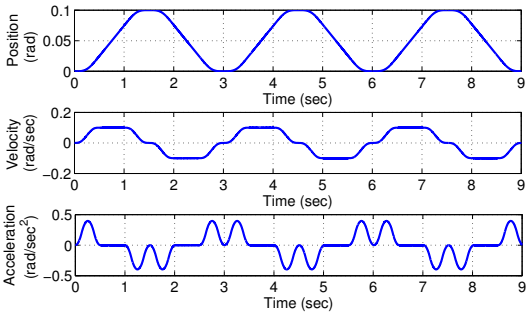

Figure 6. DESIRED LOAD SIDE TRAJECTORY

Thus, for simplicity, it is set that $\hat{\sigma}_0 = 40$ Nm·rad^{-1} and $\hat{\sigma}_1 = 0$ Nm·rad^{-1}·sec. All the identified parameters are listed in Tab. 1.

Motor Side Friction Compensation

Fig. 6 shows the desired load side trajectory in this experiment, which is designed as a fourth-order time optimal trajectory.

Feedback Friction Compensation To show the effectiveness of proposed adaptive algorithm, the estimates of friction parameters were initialized to one half of the identified values. The feedback controller gains are set as $k_p = 30$, $k_v = 0.3$, and $k_i = 1.0$ (one relaxation of Theorem 1). The adaptation gains in the feedback adaptive friction compensator (FB-A) are selected as $[\gamma_0, \gamma_1, \gamma_2, \gamma_3, \gamma_4] = [0.001, 50000, 0, 0.01, 0.001]$. For comparison, a feedforward Coulomb friction compensator (FF-C) is designed, i.e., $\hat{F} = \hat{F}_c \operatorname{sgn}\left(\dot{\theta}_{md}\right)$, using the same initial guess, $\hat{F}_C$.

Figure 7 shows the motor side and the load side tracking

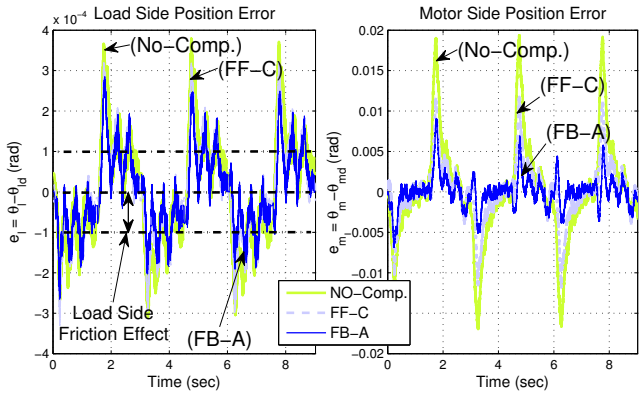

Figure 7. PERFORMANCE OF THE MOTOR SIDE COMPENSATORS (No-Comp.) [Green-Solid]: Without Friction Compensator; (FF-C) [Grey-Dash]: Feedforward Coulomb Friction Compensator; (FB-A) [Blue-Solid]: Feedback Adaptive Friction Compensator

Table 2. IMPROVEMENTS COMPARED TO THE NO-COMP. CASE

	FF-C	FB-A	FF-A	Hybrid
$\left\|\tilde{\Theta}_\ell\right\|_2$	18.30%	35.26%	37.61%	66.05%
$\left\|\tilde{\Theta}_\ell\right\|_\infty$	12.69%	32.81%	35.23%	65.77%
$\left\|\tilde{\Theta}_m\right\|_2$	45.66%	74.41%	78.53%	75.74%
$\left\|\tilde{\Theta}_m\right\|_\infty$	41.74%	68.30%	73.31%	74.78%

performance of these compensators. It is clearly seen that, motor side tracking performance is significantly improved by the FB-A method, converging to a sub-optimal stage in about 3 executions. The load side performance is slightly improved with reduced peak error. Let $\left\|\tilde{\Theta}_\ell\right\|_2$, $\left\|\tilde{\Theta}_\ell\right\|_\infty$, $\left\|\tilde{\Theta}_m\right\|_2$, and $\left\|\tilde{\Theta}_m\right\|_\infty$ denote the two-norms and ∞-norms of the load side and the motor side position errors in the last repeated execution, respectively. Table 2 shows the performance indices improved by these algorithms compared to the case without compensation (No-Comp.).

Figure 8 shows the friction estimates by FB-A, where $\hat{F}$ is fully adapted in about 3 executions. Figure 9 illustrates the adaptive friction parameter estimation process. Note that, the converged values are not exactly twice the initial values. This is because the identified values may not be exactly the actual values. Also the friction model structure is modified to adapt only three parameters. Besides, $\hat{k}_2$ is kept zero since $\hat{\sigma}_1 = 0$ and $\gamma_2 = 0$.

Feedforward Friction Compensation The modification of the proposed adaptive friction observer from the feedback form to the feedforward form is also applied in the experiment. The same controller gains, k_p, k_v, and k_i, and adaptation gains, γ_0, γ_1, and γ_2, from FB-A, are used in the feedforward compensator (FF-A). Table 2 shows that the feedforward form slightly improves the performance of the feedback form.

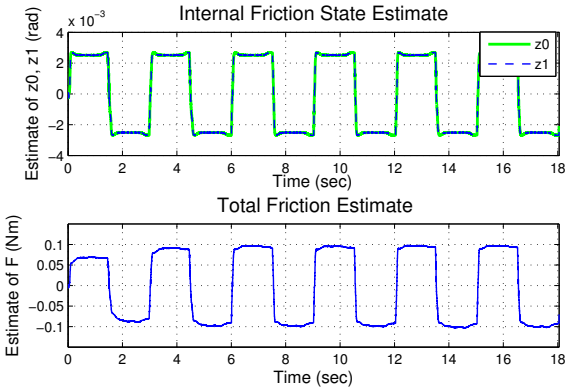

Figure 8. FRICTION ESTIMATES BY FB-A OBSERVER

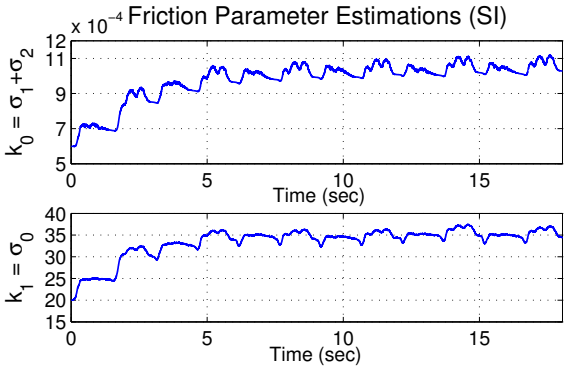

Figure 9. FRICTION PARAMETER ESTIMATIONS

Load Side Friction Compensation

The motor side compensation results (e.g., Fig. 7) show that, even if the motor side achieves good tracking performance, large position tracking error can still be observed at the load side. This indicates the necessity to implement the load side friction compensation. In Fig. 7, the oscillation in the load side position tracking error is mainly due to the transmission error [14], while the offset in the tracking error is due to the load side friction effects, which is explained in Eq. (10).

In [13], it is shown that this tracking error offset can be successfully estimated by the KKF-AG method. Therefore, this method is employed here to estimate the load side position.

To show the effectiveness of the proposed load side compensation algorithm, $\hat{r}_\ell$ was initialized to $1.0N$ where N is the reducer gear ratio. Figure 10 illustrates the performance of friction compensator enabled on both the motor side and the load side (Hybrid), i.e., the state q_1 in Fig. 3. It can be seen that the load side position tracking error offset is significantly reduced by the hybrid compensator scheme, while the motor side tracking performance is maintained at about the same level. This is also confirmed by the performance indices in Tab. 2. The load side friction compensator converges to a sub-optimal stage in less

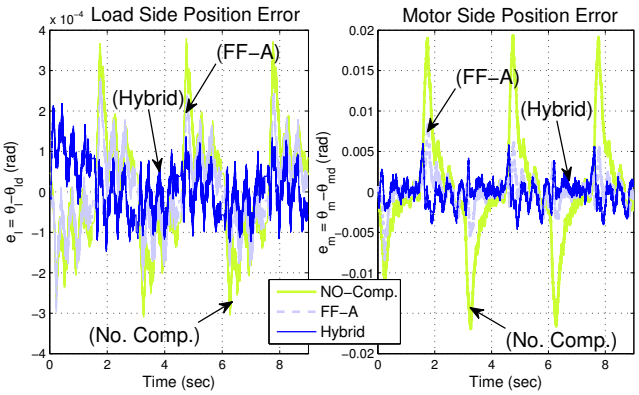

Figure 10. PERFORMANCE OF THE HYBRID COMPENSATOR (No-Comp.) [Green-Solid]: Without Friction Compensator; (FF-A) [Grey-Dash]: Feedforward Adaptive Friction Compensator at Motor Side Only; (Hybrid) [Blue-Solid]: Hybrid Compensator at the State q_1

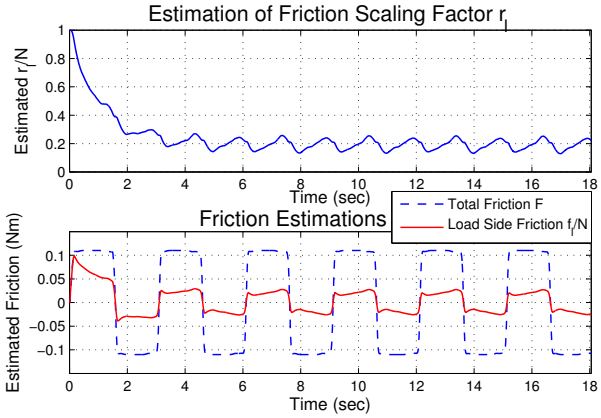

Figure 11. LOAD SIDE FRICTION ESTIMATES

than 1 execution. The convergence of estimated friction ratio $\hat{r}_\ell$ and estimated load side friction $\hat{f}_\ell$ is also confirmed in Fig. 11.

CONCLUSION

Friction compensation in indirect drive mechanisms was investigated by separating the problem into two parts, i.e., motor side and load side. The motor side compensator employed the idea of an adaptive friction observer based on the modified Lu-Gre model, while the load side compensator was implemented by injecting the load side friction estimate into the generated motor side reference. A hybrid compensator scheme was proposed to engage or disengage the load side compensator. It has been shown that additional care should be placed to the load side performance due to the load side friction in addition to the friction effects on the motor side. Experimental results demonstrated the effectiveness of the proposed scheme.

REFERENCES

[1] Canudas de Wit, C., Olsson, H., Astrom, K. J., and Lischinsky, P., 1995. "A new model for control of systems with friction". *IEEE Transactions on Automatic Control,* **40**(3), pp. 419–425.

[2] Altpeter, F., 1999. "Friction modeling, identification and compensation". PhD thesis, École Polytechnique Fédérale de Lausanne.

[3] C. Canudas de Wit, P. L., 1997. "Adaptive friction compensation with partially known dynamic friction model". *International Journal of Adaptive Control and Signal Processing,* **11**(1), pp. 65–80.

[4] Xu, L., and Yao, B., 2000. "Adaptive robust control of mechanical systems with nonlinear dynamic friction compensation". In Proceedings of the 2000 American Control Conference, Vol. 4, pp. 2595–2599.

[5] Ohnishi, K., 1987. "A new servo method in mechatronics". *Transaction of Japanese Society of Electrical Engineering,* **107-D**, pp. 83–86.

[6] Tung, E. D., Anwar, G., and Tomizuka, M., 1993. "Low velocity friction compensation and feedforward solution based on repetitive control". *Journal of Dynamic Systems, Measurement, and Control,* **115**(2A), pp. 279–284.

[7] Taghirad, H. D., and Belanger, P. R., 1998. "Modeling and parameter identification of harmonic drive systems". *Journal of Dynamic Systems, Measurement, and Control,* **120**(4), pp. 439–444.

[8] Gandhi, P. S., Ghorbel, F. H., and Dabney, J., 2002. "Modeling, identification, and compensation of friction in harmonic drives". In Proceedings of the 41st IEEE Conference on Decision and Control, Vol. 1, pp. 160–166.

[9] Soo, J., and Tomizuka, M., 2005. "Limit cycles due to friction forces in flexible joint mechanisms". In Proceedings of IEEE/ASME International Conference on Advanced Intelligent Mechatronics, pp. 723–728.

[10] Teghirad, H. D., and Belanger, P. R., 1998. "Robust friction compensator for harmonic drive transmission". In Proceedings of the 1998 IEEE International Conference on Control Applications, Vol. 1, pp. 547–551.

[11] Wen-Hong, Z., and Doyon, M., 2004. "Adaptive control of harmonic drives". In Proceedings of the 43rd IEEE Conference on Decision and Control, Vol. 3, pp. 2602–2608.

[12] Tan, Y., and Kanellakopoulos, I., 1999. "Adaptive nonlinear friction compensation with parametric uncertainties". In Proceedings of the 1999 American Control Conference, Vol. 4, pp. 2511–2515.

[13] Chen, W., 2009. "Hybrid adaptive friction compensation of indirect drive trains using joint sensor fusion". Master report, University of California at Berkeley.

[14] Cheng-Huei, H., Chun-Chih, W., and Tomizuka, M., 2008. "Suppression of vibration due to transmission error of harmonic drives using peak filter with acceleration feedback". In Proceedings of the 10th IEEE International Workshop on Advanced Motion Control, pp. 182–187.